Food Chemistry 289 (2019) 739–750

Contents lists available at ScienceDirect

Food Chemistry

journal homepage: www.elsevier.com/locate/foodchem

Relationship of phenolic composition of selected purple maize (*Zea mays* L.) genotypes with their anti-inflammatory, anti-adipogenic and anti-diabetic potential

Qiaozhi Zhang[a,b], Elvira Gonzalez de Mejia[a,*], Diego Luna-Vital[a], Tianyi Tao[c], Subhiksha Chandrasekaran[a], Laura Chatham[d], John Juvik[d], Vijay Singh[e], Deepak Kumar[e]

[a] Department of Food Science and Human Nutrition, University of Illinois at Urbana-Champaign, Urbana, IL 61801, USA
[b] College of Food Science, Northeast Agricultural University, Harbin 150030, China
[c] College of Agriculture and Biotechnology, Zhejiang University, Hangzhou, China
[d] Department of Crop Sciences, University of Illinois at Urbana – Champaign, Urbana, IL 61801, USA
[e] Department of Agricultural and Biological Engineering, University of Illinois at Urbana – Champaign, Urbana, IL 61801, USA

ARTICLE INFO

Keywords:
Phenolics
Purple maize
Inflammation
Obesity
Diabetes
Principal component analysis

ABSTRACT

This study aimed to investigate the associations between phenolic composition of selected purple maize genotypes and their anti-inflammatory, anti-adipogenic and anti-diabetic properties *in vitro*. Anthocyanin-rich water extracts (PMWs) from 20 purple maize genotypes were evaluated in RAW 264.7 macrophages and 3T3-L1 adipocytes under different conditions. Cyanidin-3-*O*-glucoside (C3G), pelargonidin-3-*O*-glucoside (Pr3G), peonidin-3-*O*-glucoside (P3G) and corresponding acylated forms were major anthocyanins in PMW, accompanied by ten tentatively identified non-anthocyanin phenolics. Correlation studies showed that C3G, P3G, and derivatives, but not Pr3G and its acylated form contributed to the biological properties of PMW. Besides anthocyanins, quercetin, luteolin, and rutin were the dominant anti-inflammatory and anti-diabetic components, in terms of down-regulating pro-inflammatory mediator production in inflamed macrophages and adipocytes, modulating diabetes-related key enzymes and improving insulin sensitivity in insulin-resistant adipocytes. Quercetin and phenolic acids, especially vanillic acid and protocatechuic acid, were closely associated with anti-adipogenic properties of PMW via inhibition of the preadipocyte-adipocyte transition.

1. Introduction

A plethora of evidence has shown that consumption of functional food ingredients could help to moderate metabolic syndrome, especially, obesity and type-2 diabetes mellitus (T2DM), two public health challenges with worldwide prevalence (Mohamed, 2014). According to the World Health Organization, overweight and obesity currently affect 39% of the adult population; and T2DM, one of the major comorbidities of obesity, was responsible for an estimated 1.6 million deaths in 2015 (World Health Organization, 2017). Intake of bioactive compounds from the diet, such as polyphenols, unsaturated fatty acids and dietary fibers have been shown to improve the obese status and T2DM-related dysfunctions (Mohamed, 2014). Anthocyanins are naturally occurring pigments widely present in many bright colored fruits, vegetables, and cereal grains. Epidemiological studies indicated that greater consumption of anthocyanin-rich foods was associated with reduced risk of metabolic diseases, like cardiovascular disease, T2DM, and certain types of cancer (Mohamed, 2014). Through different *in vitro* and *in vivo* models, several studies have shown that the anthocyanin-based extracts from various sources exhibited anti-inflammatory, anti-obesity and anti-diabetic potential, such as those from berries, purple carrot, and black soybean (Suzuki et al., 2011; Kim et al., 2012; Li, Wang, Luo, Zhao, & Chen, 2017). Some mechanisms of actions have been proposed, including their regulative effects on pro-inflammatory mediator production, preadipocyte adipogenesis, and adipocyte function, and insulin receptor signaling pathways, among others (Li, Somavat, Singh, Chatham, & de Mejia, 2017).

Moreover, anthocyanin-enriched foods with different chemical profiles are known to exhibit different health benefits. It is also noted that the phenolic composition of plants may vary among genotypes and cultivars (Wojdyło, Nowicka, Carbonell-Barrachina, & Hernández, 2016). Diversity in phytochemicals and synergistic/antagonistic effects

* Corresponding author.
E-mail address: edemejia@illinois.edu (E. Gonzalez de Mejia).

https://doi.org/10.1016/j.foodchem.2019.03.116
Received 30 November 2018; Received in revised form 18 March 2019; Accepted 21 March 2019
Available online 23 March 2019
0308-8146/

among components would impact their stability, bioavailability and metabolic pattern, yielding complex mixtures with variable bioactivities (Prior & Wu, 2006). Thus, there exists a need to understand the composition-bioactivity relationship of phenolic compounds. Based on chemical-based assays, several studies have indicated the contribution of (poly)phenols in multi-variety samples to their antioxidant and hypoglycemic properties (Wojdyło et al., 2016; Wang et al., 2015). However, biological systems, especially, cell culture models, offer cost-effective approaches to understand biological behaviors of phytochemicals and better correlate with their performance *in vivo*. Whereas, to our knowledge, very scanty information exists on the associations between phenolic distribution in food sources and their bioactive effects on obesity and T2DM-associated disorders by using cellular assays.

Currently, in addition to fruits and vegetables, colored maize (*Zea mays* L.) has emerged as an alternative source of anthocyanins, polyphenols and other phytochemicals (Paulsmeyer et al., 2017). In our previous studies, we reported that colored maize pericarp produced from a dry-milling process contained anthocyanins with suppressive effects on pro-inflammatory enzymes (Chen, Somavat, Singh, & de Mejia, 2017). It was further evidenced that anthocyanins-rich extracts from purple maize attenuated obesity-induced inflammation, adipogenesis and insulin resistance *in vitro* (Luna-Vital, Weiss, & de Mejia, 2017). Recently, we developed 20 different purple maize lines derived from the landrace Apache Red, each with a unique anthocyanin composition. In this study, each genotype was subjected to both phenolic characterization, and biochemical and cell-based approaches. Murine RAW264.7 macrophages and 3T3-L1 adipocytes were utilized, targeting obesity-associated markers in the adipose tissue. Therefore, the aim of the present study was to investigate the effect of anthocyanin-rich fractions from 20 selected purple maize genotypes on inflammation, adipogenesis, and diabetes *in vitro*, and further correlate their biological properties with their anthocyanin and phenolic composition.

2. Materials and methods

2.1. Materials

Apache Red purple maize was obtained (Siskiyou Seeds, Williams, OR) and grown for four consecutive years. Each year, harvested lines were screened for anthocyanin composition and selections made with the goal of maximizing anthocyanin diversity as described previously (Chatham, West, Berhow, Vermillion, & Juvik, 2018). In 2017, lines with unique anthocyanin profiles were planted and ears bulked from each line to produce enough maize for pericarp removal, anthocyanin extraction, and subsequent analyses. Supplementary Table S1 describes the general anthocyanin aspects associated with each line used in this study.

Both mouse cell lines (3T3-L1 preadipocytes and RAW264.7 macrophages) were obtained from the American Type Culture Collection (Manassas, VA). Dulbecco's modified Eagle medium (DMEM) was purchased from Corning cellgro® (Manassas, VA), fetal bovine serum (FBS), fetal calf serum (FCS) and penicillin-streptomycin (100×) were purchased from Gibco Life Technologies (Grand Island, NY). Primary antibody against mouse iNOS (PA1-036), COX-2 (MA5-14568), and GAPDH (MA5-15738) were obtained from Invitrogen™, Thermo Fisher Scientific (Rockford, IL). Primary antibodies against mouse PPARγ (sc-7273) and FAS (sc-48357) were obtained from Santa Cruz Biotechnology (Santa Cruz, CA). All other chemicals and reagents were products from Sigma-Aldrich (St. Louis, MO) unless otherwise indicated.

2.2. Preparation of anthocyanin-rich fractions from purple maize pericarp

Purple maize pericarp was produced at the University of Illinois at Urbana-Champaign, with a lab-scale dry-milling procedure. Extraction of anthocyanins and other phenolic compounds from the pericarp was conducted using an ASE 300 Accelerated Solvent Extraction System (Thermo Scientific). A previously established methodology using distilled water as the only solvent was performed (Luna-Vital, Li, West, West, & de Mejia, 2017). Extracts were collected, lyophilized and stored at −20 °C before analysis. The resulting freeze-dried pericarp water extract powder was referred to as purple maize anthocyanin-rich water extract (PMW) subscripted by the genotype number.

2.3. Determination of total phenolic and total anthocyanin concentrations

Each PMW was analyzed for total phenolic and total anthocyanin concentrations. The total phenolic concentration was determined using the Folin-Ciocalteu method adjusted to a microassay (Bower, Hernandez, Berhow, & de Mejia, 2014). Gallic acid was used as a standard and results were expressed as mg gallic acid equivalents (GAE) per gram of dry weight (DW). The total monomeric anthocyanin concentration was measured via the pH differential method (Lee, Durst, & Wrolstad, 2005). In brief, each PMW was dissolved in two buffer systems: 0.25 M KCl buffer, pH 1.0; and 0.40 M sodium acetate buffer, pH 4.5. 200 µL of extract solutions at each pH was transferred to a 96-well microplate, and the absorbance at 520 and 700 nm was read with a Synergy 2 multiwell plate reader (Biotek, Winooski, VT). The total monomeric anthocyanin concentration was calculated using the following equation:

$$\text{Total monomeric anthocyanin concentration (mg/L)} = (A*MW * D* 1000) /(\varepsilon*PL) * 0.45 \quad (1)$$

where: $A = (A_{520,\ pH\ 1.0} - A_{700,\ pH\ 1.0})\text{-}(A_{520,\ pH\ 4.5} - A_{700,\ pH\ 4.5})$; MW = 449.2 g/mol for cyanidin-3-glucoside (C3G); D = dilution factor; PL = constant path length, 1 cm; ε = 26900 l/(mol·cm), which is the molar extinction coefficient of C3G; 1000, conversion factor from grams to milligrams; 0.45, conversion factor from the established method to the plate reader method. The results were expressed as mg C3G equivalents per gram of DW. Values were reported as dry weight of the freeze-dried water extracts, not to the dry weight of the pericarp.

2.4. Tristimulus colorimetric measurement

The color of each PMW was measured using a HunterLab LabScan II colorimeter (Hunter Associates Laboratory, Inc., Reston, VA). The following color parameters were utilized: CIELAB values L*, a* and b*; observer/illuminant: 10° and D65 and path length of 1 cm. In brief, 2–3 mL of sample solution (1 mg/mL, in distilled water, pH 3.0, adjusted by HCl) was placed in a disposable UV–Vis cuvette, and the CIELAB values L*, a* and b* were determined. Color squares were produced by converting L*, a* and b* values to R, G and B using http://colormine.org/convert/rgb-to-lab and Microsoft PowerPoint software. The Hue angle, Chroma, and Saturation were also calculated using the following equations:

$$\text{Hue angle} = \tan^{-1}(b * /a*) \quad (2)$$

$$\text{Chroma} = \sqrt{(a^{(*2)} + b^{(*2)})} \quad (3)$$

$$\text{Saturation} = \text{Chroma}/L* \quad (4)$$

2.5. Characterization of anthocyanins and other phenolic compounds in PMW

Analysis of anthocyanins and other phenolic compounds in PMW was performed using a Dionex UltiMate® 3000 HPLC system (Thermo Fisher Scientific, Germering, Germany), coupled online to a Q-Exactive mass spectrometer (Thermo Fisher Scientific, Bremen, Germany). LC separation was performed on a Phenomenex Kinetex column (4.6 × 50 mm, 2.6 µm) with mobile phase A (0.1% formic acid in water) and mobile phase B (0.1% formic acid in acetonitrile) at a flow

rate of 0.25 mL/min. A linear gradient elution program was applied: (1) 0–3 min, 100% A; (2) 20–30 min, 0% A; (3) 30.5–36 min, 100% A. Full scan spectra were recorded under both positive and negative electrospray ionization (ESI) from *m/z* 70–1050 with a resolution of 70,000. The parameters were set as follows: capillary temperature of 257 °C; heater temperature of 415 °C; sheath gas flow rate of 45 psi; auxiliary gas flow rate of 10; sweep gas flow rate of 2.5; spray voltage of 3.5 kV for positive ESI and −2.5 kV for negative ESI, respectively. Mass spectra were acquired and interpreted using the Xcalibur™ software version 4.1.31.9 (Thermo Fisher). Phenolic compounds were identified by comparing their retention times with those available external standards and confirmed by LC-MS spectra. Quantification was achieved by injecting pure phenolic solutions with known concentrations (1 μM-1 mM for anthocyanins; 0.5 μM-500 μM for non-anthocyanin phenolics) to generate standard curves for each compound. Cyanidin-3-(6′-malonylglucoside) (C3G-Mal), pelargonidin-3-(6′-malonylglucoside) (Pr3G-Mal) and peonidin-3-(6′-malonylglucoside) (P3G-Mal) were expressed as cyanidin-3-*O*-glucoside (C3G), pelargonidin-3-*O*-glucoside (Pr3G) and peonidin-3-*O*-glucoside (P3G) equivalents, respectively. Two analytical replicates were conducted for each PMW. It is important to clarify that the values reported correspond to a freeze-dried water extract obtained from the pericarp. All values were referred to dry weight of the water extracts, not to the dry weight of the pericarp.

2.6. α-Amylase and dipeptidyl peptidase-4 inhibitory assays

Each PMW was determined for their inhibitory effects on α-amylase and dipeptidyl peptidase-4 (DPP-IV) activities. α-amylase activity inhibition was measured according to the method of Ademiluyi and Oboh (2013). DPP-IV activity inhibition was determined using a DPPIV-Glo™ protease assay kit (Cat. # G8350, Promega Corporation, Madison, WI), per the manufacturer's instructions. Each PMW was tested at different concentrations (0.05–1.0 mg/mL) and data were expressed as percentage inhibition relative to a corresponding control. Non-linear regression was performed to calculate the half-maximal inhibitory concentration (IC_{50}) of each PMW on each enzyme.

2.7. Cell culture and treatment

RAW264.7 macrophages were cultured in DMEM containing 10% (v/v) FBS, L-glutamine, sodium pyruvate, and 1% (v/v) antibiotics. 3T3-L1 preadipocytes were grown in DMEM supplemented with 10% (v/v) FCS, L-glutamine, sodium pyruvate, and 1% (v/v) antibiotics. Both cell lines were maintained at 37 °C in a fully humidified atmosphere with 5% CO_2. Fig. 1 presents the cell culture models used in this research.

2.7.1. Differentiation of 3T3-L1 preadipocytes

Differentiation of 3T3-L1 preadipocytes was performed according to the protocol of Zebisch, Voigt, Wabitsch, and Brandsch (2012). In brief, 3T3-L1 cells were seeded at a density of 6×10^3 viable cells/cm^2 (Day 0) and post-confluent cells (Day 2) were differentiated by incubation with DMEM containing 10% (v/v) FBS, 0.5 mM 3-isobutyl-1-methylxanthine, 0.25 μM dexamethasone, 2 μM rosiglitazone and 1 μg/mL insulin for 2 days. The medium was then replaced to DMEM containing 10% (v/v) FBS and 1 μg/mL insulin for another 2 days. Thereafter, the cells were maintained and replenished every other day with 10% FBS-DMEM until Day 10 when 80–90% of the cells exhibited typical adipocyte morphology.

2.7.2. Effect of PMW on LPS-induced RAW264.7 macrophages and TNF-α-induced 3T3-L1 adipocytes

The anti-inflammatory potential of PMW was evaluated in both RAW264.7 macrophages and 3T3-L1 adipocytes (Fig. 1A). RAW264.7 macrophages were seeded at a density of 3×10^4 viable cells/cm^2. Serum-starved cells were pretreated with 1 mg/mL of each PMW for 4 h, after which, 1 μg/mL lipopolysaccharides (LPS) was added to the cells and further stimulated for 24 h. The cell culture supernatant was collected for NO and cytokine measurements; cell lysate was collected for western blotting.

3T3-L1 preadipocytes were seeded and differentiated according to the conditions in Section 2.7.1. Fully differentiated adipocytes were incubated with 1 mg/mL of each PMW, along with 10 ng/mL of TNF-α for 24 h. Thereafter, the cell supernatant was harvested for adipokine determination.

2.7.3. Effect of PMW during 3T3-L1 preadipocyte differentiation and in mature adipocytes

The anti-adipogenic potential of PMW was investigated both in preadipocyte-adipocyte transition and in mature adipocytes (Fig. 1B). 3T3-L1 preadipocytes were bedded and induced to differentiation as indicated in Section 2.7.1. 1 mg/mL of each PMW was included in the cell culture media during the differentiation process until Day 10 when the cell lysate was harvested for western blotting.

Lipolysis under basal conditions was assessed in mature 3T3-L1 adipocytes. 3T3-L1 preadipocytes were seeded and differentiated (Section 2.7.1). On Day 10, the fully differentiated adipocytes were treated with 1.0 mg/mL of each PMW for 24 h. Afterwards, the cell supernatant and cell lysates were harvested for lipolysis assays.

2.7.4. Potential of PMW in TNF-α-induced insulin resistant 3T3-L1 adipocytes

The anti-diabetic potential of PMW was evaluated in insulin-resistant 3T3-L1 adipocytes (Fig. 1C). 3T3-L1 preadipocytes were seeded and differentiated as mentioned in Section 2.7.1. To induce insulin resistance in adipocytes, fully differentiated cells were incubated with 10 ng/mL of TNF-α for 4 days, with refreshing the culture media every 24 h. A reduction in insulin-mediated glucose uptake (by using the assay described below in Section 2.12) was confirmed after this period. On Day 14, after full differentiation and induction, 1 mg/mL of each PMW was added to the cells and further incubated for 24 h. Following treatment, living cells were analyzed for real-time assays.

2.8. Impact of PMW on NO, cytokine and adipokine production

Nitric oxide (NO) production in the RAW 264.7 macrophage supernatant was determined using the Griess reagent (Cat. # G4410), per the manufacturer's instructions. In brief, 100 μL of the supernatant was combined with 100 μL of Griess reagent in a 96-well microplate. After standing at room temperature for 15 min, the absorbance was recorded at 540 nm. $NaNO_2$ (1.25–50 μM) was used as a standard to generate a standard curve.

Macrophage-derived cytokines, namely, prostaglandin E_2 (PGE_2, Cat. # 500141, Cayman Chemical, Ann Arbor, MI), TNF-α (Cat. # DY410, R&D systems, Minneapolis, MN), and interleukin-6 (IL-6, Cat. # DY406, R&D systems); adipocyte-derived adipokines, including monocyte chemoattractant protein-1 (MCP-1, Cat. # DY479, R&D systems), adiponectin (Cat. # KMP0041, Invitrogen™, Thermo Fisher Scientific, Rockford, IL), and leptin (Cat. # DY498, R&D systems) were quantified using the specified commercial ELISA kits, according to the supplier's instructions.

2.9. Effect of PMW on lipid accumulation during preadipocyte adipogenesis

Intracellular lipid accumulation was determined using Oil Red O staining according to the method of Luna-Vital et al. (2017). 3T3-L1 preadipocytes were seeded and induced to differentiation as described in Section 2.7.1. During the differentiation process, 1 mg/mL of each PMW was incorporated in the cell culture media and lipid staining was performed on Day 10. An Oil red O stock solution was prepared by stirring 0.5% (w/v) Oil Red O in isopropanol overnight and filtered (0.22 μm, Thermo Fisher Scientific). Adipocytes were washed with PBS,

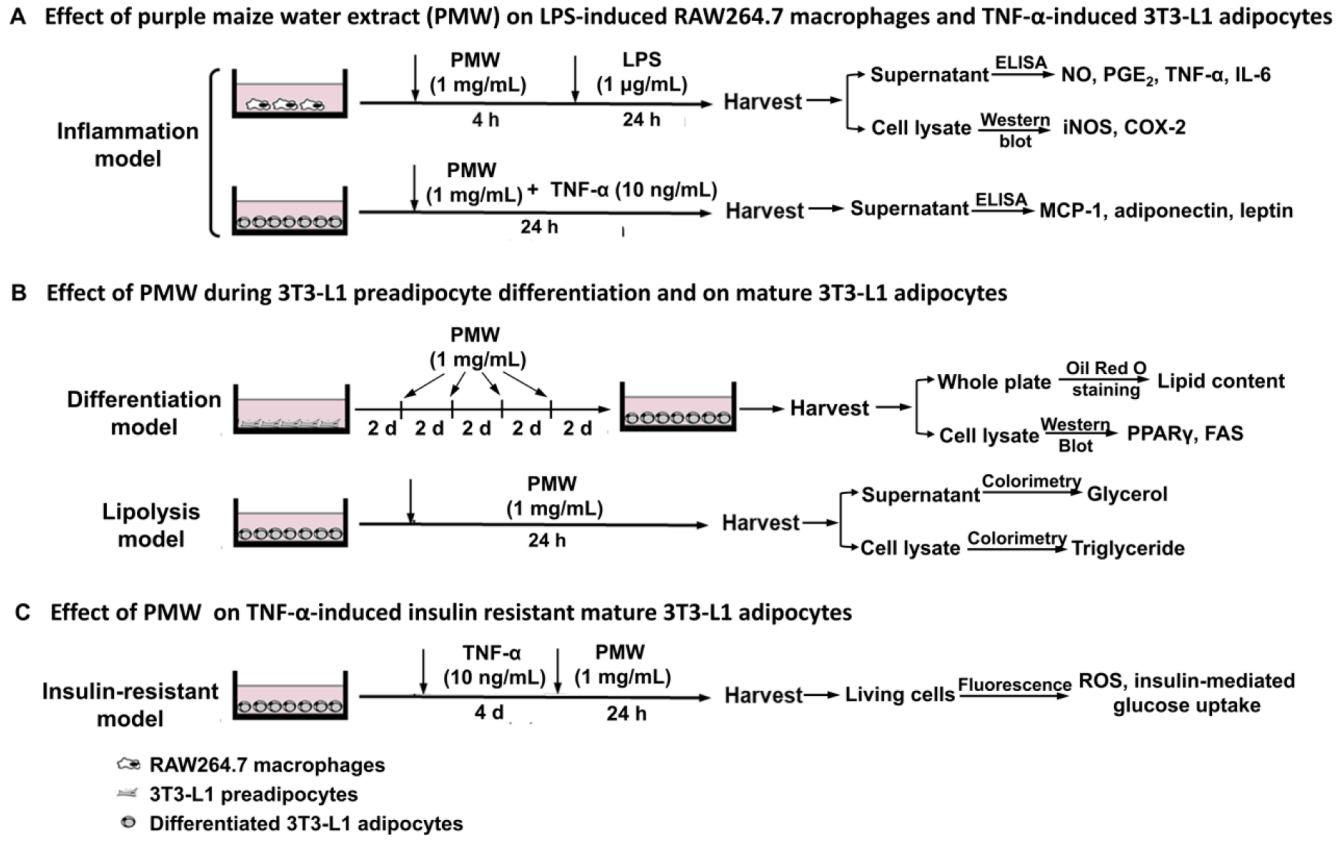

Fig. 1. Illustration of the cell culture models used.

fixed with 10% formaldehyde and stained with an Oil Red O working solution for 10 min at room temperature. Afterwards, the plates were washed extensively with deionized water, dried and photographed. Intracellular lipid content was quantified by dissolving the staining in isopropanol and read for absorbance at 500 nm in a spectrophotometer.

2.10. Assessment of lipolysis in mature 3T3-L1 adipocytes

The lipolysis under basal conditions was assessed in mature 3T3-L1 adipocytes. Briefly, 3T3-L1 preadipocytes were seeded, differentiated and treated with each PMW as indicated in 2.7.1 and 2.7.3. Following 24 h treatment, the cell supernatant was tested for glycerol content using a glycerol assay kit (Cat. # MAK117) and cell lysate was harvested for triacylglycerol (TG) quantification with a triglyceride colorimetric assay kit (Cat. # 10010303, Cayman Chemical, Ann Arbor, MI).

2.11. Intracellular ROS generation in insulin-resistant 3T3-L1 adipocytes

Intracellular ROS generation in insulin-resistant 3T3-L1 adipocytes was determined according to the method of Luna-Vital et al. (2017), using 2′,7′-dichlorofluorescein diacetate (DCFH-DA) as a probe. In brief, 3T3-L1 preadipocytes were cultured, differentiated and induced to insulin resistance in black, clear-bottom, 96-well plates (Section 2.7.1 and 2.7.4.). On Day 14, after full differentiation and induction, the adipocytes were treated with 1.0 mg/mL of each PMW for 24 h. Following treatment, 40 μM DCFH-DA was added to the cells and further incubated at 37 °C for 60 min in the dark. Then, the cells were washed twice with HBSS and fluorescence intensity was recorded at an excitation/emission wavelength of 485 nm/535 nm, respectively.

2.12. Glucose uptake in insulin-resistant 3T3-L1 adipocytes

Glucose uptake in insulin-resistant 3T3-L1 adipocytes was evaluated using the 2-Deoxy-2-[(7-nitro-2,1,3-benzoxadiazol-4-yl)amino]-D-glucose (2-NBDG) assay as previously described (Alonso-Castro & Salazar-Olivo, 2008). In brief, 3T3-L1 preadipocytes were seeded, differentiated and induced in black, clear-bottom, 96-well plates (Section 2.7.1 and 2.7.4). On Day 14, fully differentiated and induced adipocytes were treated with 1.0 mg/mL of each PMW for 24 h. Thereafter, the cells were starved for 4 h and stimulated with 100 nM insulin for an extra 30 min. Subsequently, 100 μM 2-NBDG in glucose-free DMEM was added to the cells and further maintained at 37 °C for 60 min in the dark. The cells were then washed twice with HBSS and fluorescence intensity was determined at an excitation wavelength of 485 nm and an emission wavelength of 535 nm, respectively.

2.13. Western blot analysis of protein expression levels related to inflammation and adipogenesis

RAW264.7 macrophages or 3T3-L1 adipocytes were seeded and treated as described in Sections 2.7.2–2.7.4. Treated cells were washed with PBS, lysed in ice-cold RIPA buffer and centrifuged at 10,000*g*, 4 °C for 10 min to remove cell debris. Proteins (20 μg/lane) were subjected to 4–20% gradient SDS−polyacrylamide gels and transferred onto polyvinylidene difluoride membranes. After blocking with 3% (w/v) nonfat dry milk in 0.1% Tris-buffered saline-Tween 20, the membranes were incubated with primary antibodies (1:500) at 4 °C overnight. The membranes were then incubated with horseradish peroxidase-conjugated secondary antibody (1:2500, GE Healthcare, Buckinghamshire, UK) for 2 h and blots were developed using an enhanced chemiluminescence kit (GE Healthcare, Buckinghamshire, UK). Pictures were taken on a GelLogic 4000 Pro Imaging System (Carestream Health, Inc., Rochester, NY). The intensity of each band was normalized to that of

GAPDH and results were expressed as expression level relative to a control.

2.14. Statistical analysis

All data were expressed as the mean ± standard deviations (SD) from at least three independent experiments unless otherwise specified. One-way analysis of variance (ANOVA), followed by Tukey's post hoc test was used to determine the differences among mean values. Differences were considered to be statistically significant when $p < 0.05$. Pearson correlation and principal component analysis (PCA) were performed to correlate phenolic compositions of PMW with their biological properties. A two-step cluster analysis was also conducted to determine the associations among genotypes. IBM SPSS Statistics Version 25.0 (SPSS Inc., Chicago, IL, USA) was used for all statistical analysis.

3. Results and discussion

3.1. Chemical characterization and phenolic composition of PMW

Representative kernel samples of the 20 purple maize genotypes are presented in Fig. 2A. As seen, the landrace Apache Red exhibited pigmented kernels with purplish-red seed coat. It was previously evidenced that, in purple maize, the pigments predominantly were located in the pericarp (Li et al., 2017). Hence, in this study, the pericarp was removed from each genotype and subsequently used for anthocyanin extraction. Yield of pericarp from kernels is shown in Table 1 and mass balance during dry milling process is given in Supplementary Table S2. Total phenolic and total anthocyanin concentrations in all 20 PMW are first determined and shown in Table 1. The total phenolic contents (TPC) in PMW varied from 69.1 to 225.1 mg GAE/g DW, and total anthocyanin contents (TAC) were from 12.8 to 93.5 mg C3G equivalents/g DW. Cuevas-Montilla, Hillebrand, Antezana, and Winterhalter (2011) reported that the TPC and TAC present in nine Bolivian purple maize varieties was within 3.1–8.2 mg GAE/g maize, and 0.02–0.7 mg C3G equivalents/g maize, respectively. Similar levels of TPC were observed in six colored maize genotypes (4.5–10.5 mg GAE/ g maize), but lower TAC values were registered (0.003–0.7 mg C3G equivalents/g maize) (Žilić, Serpen, Akıllıoğlu, Gökmen, & Vančetović, 2012). Mazewski, Liang, and de Mejia (2017) extracted anthocyanins from purple maize pericarp using water and ethanol. TAC value in the resulting powder was 92.3 mg C3G equivalents/g extract. Haggard et al. (2018) extracted anthocyanins from pericarps of nine purple maize varieties using high-pressured water (1500 psi). TPC levels obtained were 44.4–179.4 mg GAE/g extract and TAC values in a beverage model (0.2–1.0 mg/mL) were 24.7–97.9 μg C3G equivalents/mL. Monroy, Rodrigues, Sartoratto, and Cabral (2016) used supercritical CO_2, ethanol and water to sequentially extract bioactive compounds from purple maize pericarp. The TPC and TAC levels reported were 278–302 mg GAE/g extract and 41.3–63.1 mg C3G equivalents/g extract, respectively. Yang and Zhai (2010) applied microwave-assisted extraction on purple maize cob and registered an optimal TAC level of 1.9 mg C3G equivalents/g cob. Also, Chen, Yang, Mou, and Kong (2018) used ultrasound-assisted extraction conditions for purple maize anthocyanins and reported the highest TAC value of 3.6 mg C3G equivalents/g bran. These widely ranged results are due to the extraction procedures, analytical methods, reporting of results either per whole food, dry extract, dry cods or dry bran, geographical origins and sample genotypes used. The reason for the high level of TPC and TAC in the current research is due to the extraction method used and the reporting of the results as per dry water extract (not dry pericarp). We used high-pressured water (1500 psi) to repeatedly flushing finely grounded pericarp in the extraction cell for 5 times, 5 min each (each time also included preheating to 50 °C and nitrogen purge for 60 s in the end). Compared with traditional solvent/acidic water extraction at ambient pressure, the current method extracted a greater content of water-soluble phenolic components from the pericarp.

When calculating our results based on dry weight of pericarp and whole maize (Supplementary Table S3), TPC and TAC (both extractable) values in the pericarp were 1.5–12.9 mg GAE/g pericarp and 0.2–7.8 mg C3G equivalents/g pericarp, consistent with those reported by Chatham et al. (2018) (TAC in purple and red maize: 0.2–6.1 mg/g pericarp). Besides, based on pericarp yield (Table 1), TPC and TAC levels in dry weight of whole maize were 0.2–1.3 mg GAE/g maize and 0.02–0.5 mg C3G equivalents/g maize. Hu and Xu (2011) reported that TPC and TAC in pigmented maize were 2.6–3.9 mg GAE/g maize and 0.06–2.8 mg C3G equivalents/g maize, respectively. Moreover, Zhao et al. (2008) registered that five Chinese purple maize hybrids contained 2.5–4.9 mg GAE/g maize and 0.2–3.0 mg C3G equivalents/g maize. By using Pearson correlation analysis, a non-significant correlation was found between the TPC and TAC values ($p > 0.05$), indicating the presence of other phenolic compounds in the extracts.

The color squares of each PMW are displayed in Table 1, and the detailed color parameters, including L*, a*, b*, Hue angle, Chroma, and Saturation can be retrieved from Supplementary Table S4. Overall, PMW exhibited colors from earth red to red-violet, with Hue angles comprising from −84.9 to 73.8. The highest Chroma value, an indicator of the color intensity, was recorded in PMW_{13} (57.0), followed by PMW_4 (55.8), PMW_{19} (47.4), and PMW_{15} (41.5), respectively. A significant correlation was observed between Chroma and TAC ($r = 0.781$, $p < 0.0001$), suggesting that anthocyanins contributed to the color strength. A similar relationship was demonstrated by Haggard et al. (2018) (Chroma *vs.* TAC, $r = 0.788$), where the colored maize pigments were used in a beverage model.

The composition of phenolic compounds in each PMW is given in Table 1 (for monomeric anthocyanins) and Supplementary Table S5 (for condensed dimer and other phenolics). Selection of the tentatively identified phenolics was based on our previous study on colored maize anthocyanin characterization (Haggard et al., 2018), and those monomeric phenolics commonly reported in other pigmented maize cultivars (Harakotr, Suriharn, Tangwongchai, Scott, & Lertrat, 2014; Lao & Giusti, 2016). Information of the retention time, polarity and MS ions of each selected compound is summarized in Supplementary Table S6. It is known that mainly three types of anthocyanidins are present in maize: cyanidin, pelargonidin and peonidin, and the derivatives differed in hydroxylation or methoxylation forms of the phenyl group on the aromatic B ring (Paulsmeyer et al., 2017). Here, total seven anthocyanins were determined, including three glycosides (C3G, Pr3G, and P3G), three acylated glycosides (C3G-Mal, Pr3G-Mal, and P3G-Mal), and a flavanol–anthocyanin dimer (catechin-cyanidin-3,5-diglucoside). Representative MS spectra of the three anthocyanin glycosides are presented in Fig. 2B. In general, our results well matched the anthocyanin patterns reported for pigmented maize by Paulsmeyer et al. (2017) and Lao and Giusti (2016), where glucose was found to be the major glycoside and modification was most seen by acylation in the form of malonyl. Moreover, the concentrations found in this study compared with the literature using extracts of phenolics in dry basis. Luna-Vital et al. (2017) registered that anthocyanin-rich extract from purple maize pericarp contained 16.0 mg C3G/g extract and 6.9 mg P3G/g extract. As shown in Fig. 2C, two heat maps intuitively visualizing the phenolic profiles of all 20 extracts are shown. Apparently, distribution of the six monomeric anthocyanins varied significantly among genotypes. The amounts of C3G, Pr3G and P3G and their corresponding derivatives ranged within 0.2–14.2, 0.02–7.5, and 0.1–3.6 mg/g DW, respectively. Also, a strong correlation was found between TAC and the content of C3G ($r = 0.744$, $p < 0.001$), C3G-Mal ($r = 0.654$, $p < 0.01$), P3G ($r = 0.782$, $p < 0.0001$) and P3G-Mal ($r = 0.755$, $p < 0.001$).

With respect to other phenolics, five phenolic acids (*o*-coumaric acid, caffeic acid, vanillic acid, protocatechuic acid, and ferulic acid) and five flavonoids (rutin, luteolin, quercetin, naringenin, and

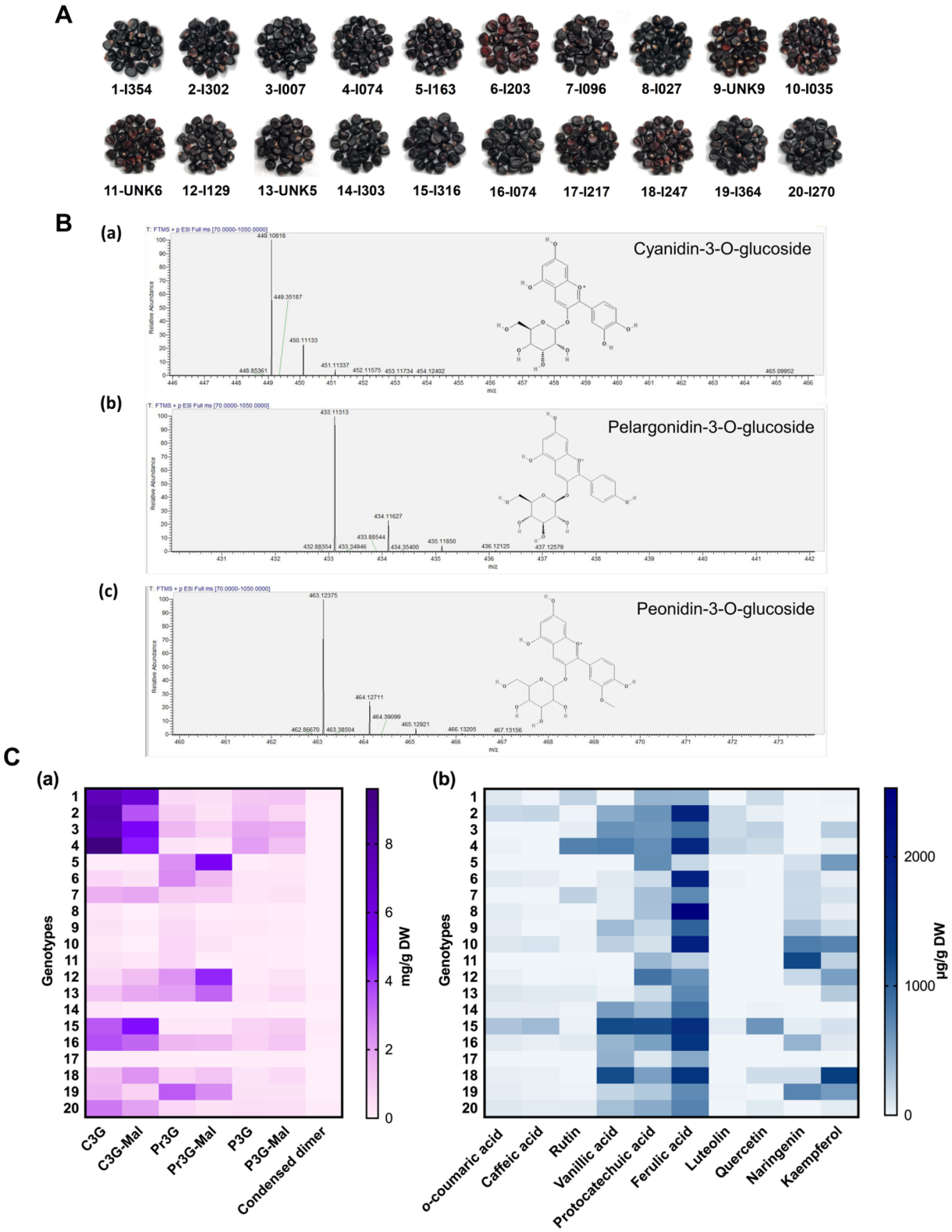

Fig. 2. (A) Kernel samples of the 20 purple maize genotypes; (B) Representative MS spectra of (a) C3G, (b) Pr3G, and (c) P3G; (C) Heat map of the chemical composition of (a) anthocyanins and (b) other phenolic compounds in PMW. C3G, cyanidin-3-*O*-glucoside; Pr3G, pelargonidin-3-*O*-glucoside; P3G, peonidin-3-*O*-glucoside; C3G-Mal, cyanidin-3-(6′-malonylglucoside); Pr3G-Mal, pelargonidin-3-(6′-malonylglucoside); P3G-Mal, peonidin-3-(6′-malonylglucoside); Condensed dimer was identified as catechin-cyanidin-3,5-diglucoside. (For interpretation of the references to color in this figure legend, the reader is referred to the web version of this article.)

kaempferol) were identified in PMW. Again, these phenolic compounds are differentially distributed among genotypes. Overall, besides anthocyanins, ferulic acid (186.2–2530.8 μg/g DW) dominated the phenolic profiles of PMW, followed by protocatechuic acid (80.7–1159.5 μg/g DW) and vanillic acid (0–1168.7 μg/g DW), and to lesser extents, kaempferol (0–1270.3 μg/g DW) and naringenin

Table 1
Characterization and anthocyanin composition of purple maize pericarp water extracts.

Genotypes	Yield (g pericarp/ 100 g dry maize)	Total phenols (mg GAE/g DW)	Total anthocyanins (mg C3G equivalents/ g DW)	Anthocyanin glycosides (mg/g DW)			Acylated anthocyanin glycosides (mg/g DW)			Color*
				C3G	Pr3G	P3G	C3G-Mal	Pr3G-Mal	P3G-Mal	
1	5.8	151.1 ± 0.2^{d}	43.4 ± 4.7^{cdef}	7.40 ± 0.06^{a}	0.61 ± 0.01^{h}	1.11 ± 0.00^{d}	**6.33** ± 0.10^{a}	0.45 ± 0.00^{gh}	**1.21** ± 0.01^{bc}	
2	6.7	154.7 ± 2.0^{d}	72.2 ± 2.9^{b}	**7.97** ± 0.06^{a}	0.99 ± 0.01^{f}	**1.24** ± 0.00^{c}	3.51 ± 0.01^{d}	0.42 ± 0.01^{h}	0.76 ± 0.01^{e}	
3	4.9	126.0 ± 5.4^{fg}	**74.9** ± 3.9^{b}	**7.67** ± 0.27^{a}	1.48 ± 0.04^{e}	**1.87** ± 0.02^{b}	**5.08** ± 0.04^{b}	0.85 ± 0.02^{fg}	**1.70** ± 0.02^{a}	
4	5.3	152.5 ± 1.0^{d}	**93.5** ± 3.9^{a}	**9.61** ± 0.06^{a}	0.33 ± 0.00^{i}	**2.05** ± 0.01^{a}	4.56 ± 0.08^{c}	0.17 ± 0.01^{hi}	**1.27** ± 0.05^{b}	
5	6.9	69.1 ± 1.0^{l}	40.8 ± 1.2^{ef}	0.07 ± 0.00^{d}	**2.34** ± 0.01^{c}	0.08 ± 0.00^{m}	0.15 ± 0.00^{k}	**5.15** ± 0.10^{a}	0.19 ± 0.00^{j}	
6	7.1	115.0 ± 1.0^{hi}	48.7 ± 5.2^{cde}	0.66 ± 0.02^{cd}	**2.49** ± 0.04^{b}	0.30 ± 0.00^{hi}	0.37 ± 0.04^{j}	1.44 ± 0.40^{e}	0.27 ± 0.00^{i}	
7	7.4	141.1 ± 1.0^{e}	38.5 ± 3.9^{ef}	1.66 ± 0.06^{bcd}	0.97 ± 0.05^{f}	0.27 ± 0.02^{i}	1.89 ± 0.05^{g}	0.94 ± 0.01^{f}	0.41 ± 0.00^{gh}	
8	9.0	108.0 ± 0.7^{j}	17 ± 1.2^{h}	0.26 ± 0.00^{d}	0.40 ± 0.01^{i}	0.08 ± 0.00^{lm}	ND	0.001 ± 0.00^{i}	0.02 ± 0.00^{l}	
9	7.3	**184.4** ± 4.8^{b}	21.2 ± 4.7^{gh}	0.40 ± 0.02^{cd}	0.62 ± 0.01^{h}	0.18 ± 0.00^{j}	0.12 ± 0.00^{k}	0.21 ± 0.00^{hi}	0.09 ± 0.00^{k}	
10	8.0	132.7 ± 0.7^{f}	21.7 ± 2.3^{gh}	0.19 ± 0.02^{d}	0.67 ± 0.03^{h}	0.06 ± 0.00^{m}	ND	0.33 ± 0.00^{hi}	0.02 ± 0.00^{l}	
11	10.1	119.6 ± 0.9^{gh}	15.8 ± 3^{h}	0.38 ± 0.00^{cd}	0.68 ± 0.01^{h}	0.09 ± 0.00^{lm}	0.25 ± 0.00^{jk}	0.01 ± 0.00^{i}	0.03 ± 0.00^{kl}	
12	7.3	111.7 ± 3.3^{ij}	47.2 ± 5.2^{cde}	0.65 ± 0.01^{cd}	2.28 ± 0.04^{c}	0.14 ± 0.00^{jk}	1.34 ± 0.04^{h}	**4.38** ± 0.12^{b}	0.36 ± 0.00^{h}	
13	6.4	80.8 ± 0.5^{k}	**75.7** ± 2^{b}	1.18 ± 0.03^{bcd}	2.02 ± 0.02^{d}	0.28 ± 0.00^{hi}	1.81 ± 0.02^{g}	**3.21** ± 0.10^{c}	0.57 ± 0.01^{f}	
14	6.9	152.5 ± 0.9^{d}	23 ± 4.8^{gh}	0.29 ± 0.01^{d}	0.02 ± 0.00^{k}	0.12 ± 0.00^{kl}	0.07 ± 0.00^{k}	0.01 ± 0.00^{i}	0.03 ± 0.00^{kl}	
15	9.8	**190.4** ± 2.0^{b}	50.4 ± 3.1^{cde}	5.35 ± 0.00^{b}	0.21 ± 0.01^{j}	0.77 ± 0.02^{e}	**4.74** ± 0.01^{c}	0.24 ± 0.00^{hi}	0.97 ± 0.01^{d}	
16	9.4	165.3 ± 4.0^{c}	54.4 ± 2.1^{c}	3.62 ± 0.14^{b}	1.49 ± 0.01^{e}	0.81 ± 0.00^{e}	3.20 ± 0.01^{e}	1.40 ± 0.06^{e}	1.15 ± 0.03^{c}	
17	10.5	110.4 ± 1.0^{ij}	12.8 ± 3^{h}	0.09 ± 0.00^{d}	0.01 ± 0.00^{k}	0.06 ± 0.00^{m}	0.08 ± 0.00^{k}	0.01 ± 0.00^{i}	0.06 ± 0.00^{kl}	
18	7.0	**229.1** ± 0.6^{a}	32.1 ± 2.8^{fg}	1.36 ± 0.06^{bcd}	0.83 ± 0.04^{g}	0.31 ± 0.01^{h}	2.28 ± 0.04^{f}	1.19 ± 0.01^{ef}	0.62 ± 0.02^{f}	
19	7.4	141.2 ± 1.7^{e}	54.1 ± 3.1^{cd}	1.52 ± 0.05^{bcd}	**3.39** ± 0.04^{a}	0.37 ± 0.00^{g}	0.83 ± 0.03^{i}	2.45 ± 0.02^{d}	0.37 ± 0.01^{h}	
20	9.6	150.1 ± 0.6^{d}	43.2 ± 1.5^{de}	2.83 ± 0.05^{bc}	0.67 ± 0.03^{h}	0.54 ± 0.02^{f}	1.98 ± 0.12^{g}	0.44 ± 0.02^{h}	0.47 ± 0.01^{g}	

DW, dry weight of water extract; GAE, gallic acid equivalents; ND, not detected; C3G, cyanidin-3-*O*-glucoside; Pr3G, pelargonidin-3-*O*-glucoside; P3G, peonidin-3-*O*-glucoside; C3G-Mal, cyanidin-3-(6′-malonylglucoside); Pr3G-Mal, pelargonidin-3-(6′-malonylglucoside); P3G-Mal, peonidin-3-(6′-malonylglucoside).
Values are expressed as the mean ± SD from three replicates for total phenolic and anthocyanin concentrations, and two replicates for anthocyanin composition. Different superscript letters indicate significant difference within the same column ($p < 0.05$, Tukey's test) and the three highest values are highlighted in bold.
* Color parameters including L*, a*, b*, Hue angle, Chroma, and Saturation can be referred in Supplementary Table S4.

(0–1197.7 μg/g DW) (Supplementary Table S5 and Fig. 2C). Similarly, Harakotr et al. (2014) characterized phytochemicals of purple wax maize kernel and found that ferulic acid and protocatechuic acid topped the non-anthocyanin phenolics. Moreover, ferulic acid and protocatechuic acid, both being major metabolites of anthocyanins, have been portrayed with beneficial effects in reducing metabolic diseases *in vitro* and *in vivo* (Mancuso & Santangelo, 2014; Min, Ryu, & Kim, 2010); Kaempferol and naringenin are known as dietary flavonoids with various biological properties, like antioxidant, anti-inflammatory and anti-carcinogenic activities (González-Gallego, García-Mediavilla, Sánchez-Campos, & Tuñón, 2014; Hsu & Yen, 2006). Taken together, these results confirmed purple maize pericarp as a promising source of phytochemicals and can be regarded as food components with health-promoting features.

3.2. Potent anti-inflammatory effect of PMW in LPS-activated RAW 264.7 macrophages and TNF-α-induced 3T3-L1 adipocytes

After a 24-h incubation, none of the twenty PMW significantly reduced the cell viability (CV) of RAW264.7 macrophages except for PMW_{15} (-52.2%, compared with untreated control (NC), $p < 0.05$) (Supplementary Figure S1). As for 3T3-L1 adipocytes, $PMW_{12\text{-}15}$ and $PMW_{17\text{-}19}$ exhibited cytotoxic effects, reducing the CV by 18.2–68.7%, when compared to the NC ($p < 0.05$). Induction of apoptosis constitutes a possible explanation since several phenolics present in PMW have been reported with apoptosis-inducing effects in 3T3-L1 pre-adipocytes and adipocytes (Hsu & Yen, 2006). To confirm this hypothesis, the expression level of cytochrome *C*, a pro-apoptotic protein released from mitochondria during the initial stages of apoptosis, was evaluated in adipocytes after treating with each aforementioned PMW (Supplementary Figure S2). As seen, with respect to the NC, activation of cytochrome *C*-mediated apoptotic events was observed (-8.3 to 181.0%; Cytochrome *C* expression *vs.* CV, $r = -0.701$, $p < 0.05$), indicating apoptosis as a partial mechanism through which certain PMW reduced CV in adipocytes. Besides, synergistic effects among phenolics and the presence of other water-soluble compounds could also play a role in the decreased viability in genotypes 15, 17 and 18 (Yang et al., 2008). It would be interesting to investigate further the underlying pro-apoptotic mechanism of specific genotypes. However, that was not deeply explored since it was not the focus of the present study. To avoid interference of cell growth, the following results were herein corrected to the cellular protein content or appropriate loading protein control was used, unless otherwise specified.

In obese subjects, progression of adipose tissue dysfunction and adipocyte hypertrophy were observed, resulting in elevated secretion of circulating fatty acids, hormones and pro-inflammatory cytokines (Weisberg et al., 2003). Moreover, macrophages infiltrate into the adipose tissue and exert impact on adipocyte metabolism, which is another key feature in the development of obesity-associated insulin resistance and T2DM (Mraz & Haluzik, 2014). It is known that regulation of pro-inflammatory mediator production serves as a key mechanism of inflammation control. LPS, a major endotoxin derived from the gut microbiota, and TNF-α, a crucial cytokine that initiates adipocyte dysfunction, are considered as inflammatory stimuli in the adipose tissue. As seen in Fig. 3A, compared to the LPS control, PMW decreased the production of NO by 13.0–59.5%. Likewise, the PGE_2 level in activated macrophages was also down-regulated by PMW, except for PMW_3, by 10.4–87.0% (Fig. 3B). Moreover, secretion levels of TNF-α and IL-6, two macrophage factors that aggravate adipocyte inflammation, were also regulated by PMW with varying degrees from −9.7 to −64.8% and 2.5 to −60.1%, respectively (Fig. 3C and D). In obese subjects, an enhanced plasma concentration of MCP-1 was observed, and in rodent models, MCP-1 was implied to contribute to the macrophage recruitment in adipose tissue and to the development of insulin resistance in obesity (Kanda et al., 2006). As seen in Fig. 3E, treatment with TNF-α alone dramatically exacerbated the MCP-1 secretion, while all twenty PMW, except for PMW_3, PMW_5, and $PMW_{8\text{-}9}$ statistically down-regulated its level by 21.2–50.3% ($p < 0.05$). Moreover, adiponectin is well-established as an anti-inflammatory mediator as indicated by Kusminski, Bickel, and Scherer (2016). In the present study, it was

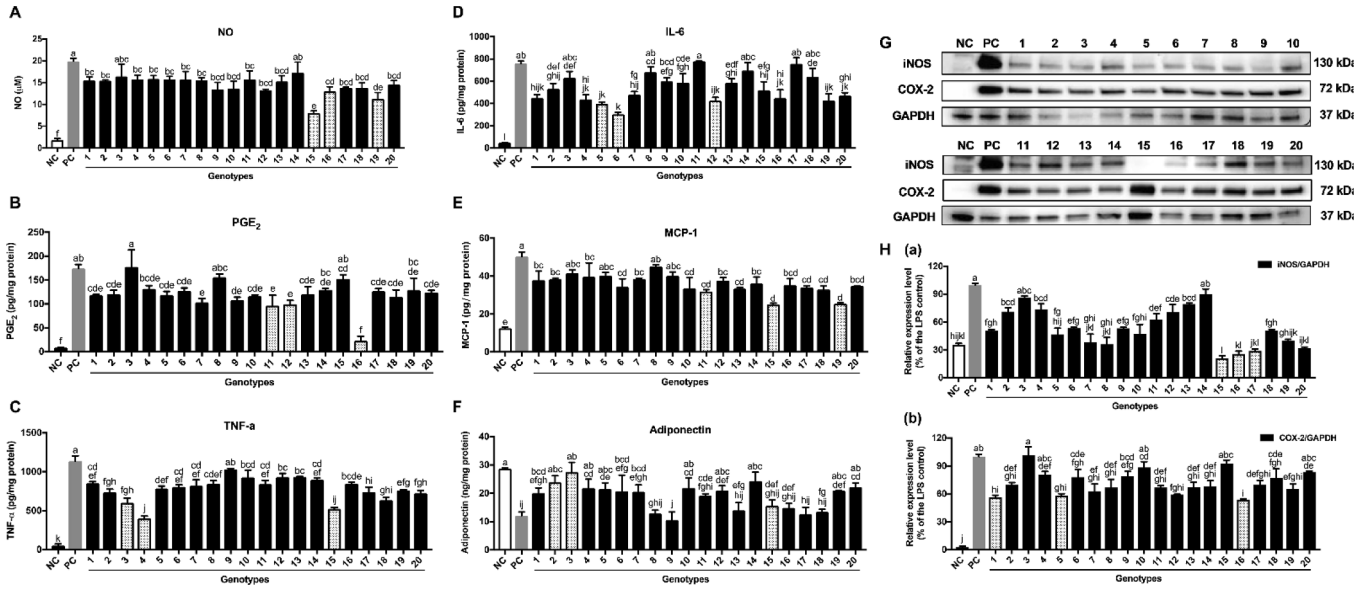

Fig. 3. Impact of PMW on (A) NO, (B) PGE_2, (C) TNF-α and (D) IL-6 production in LPS-stimulated macrophages, (E) MCP-1, (F) Adiponectin in TNF-α-induced adipocytes, and (G)-(H) iNOS and COX-2 expression in LPS-activated macrophages. RAW264.7 macrophages were pretreated with 1.0 mg/mL of each PMW for 4 h, followed by activation with 1 μg/mL of LPS for 24 h. 3T3-L1 adipocytes were incubated with 1.0 mg/mL of each PMW along with 10 ng/mL of TNF-α for 24 h. Values are expressed as the mean ± SD from three independent replicates in (A)-(F), and two independent replicates in (G)-(H). Bars with different letters indicate statistical difference ($p < 0.05$, Tukey's test) and the three most effective genotypes are filled with spotted pattern.

significantly diminished in TNF-α-induced adipocytes (Fig. 3F, $p < 0.05$). PMW_{1-7}, PMW_{10}, PMW_{12}, PMW_{14}, and PMW_{19-20} statistically up-regulated the adiponectin secretion in inflamed adipocytes by 29.1–127.2%. As for leptin, a pro-inflammatory adipokine with lipolytic action (Kusminski et al., 2016), a statistical increase was noticed upon TNF-α induction (Supplementary Figure S3, $p < 0.05$); PMW reversed this induced leptin level, while non-significant differences were observed among genotypes ($p > 0.05$).

It was further confirmed by western blotting that PMW (PMW_3 not included) inhibited the expression levels of iNOS and COX-2 by 10.2%-79.2% and 7.6%-46.1%, respectively (Fig. 3G and H). Highly expressed iNOS and COX-2 are responsible for the prolonged excretion of NO and PGE_2 at injured sites, and expectedly, a strong correlation was observed between NO and iNOS ($r = 0.556$, $p < 0.05$), and PGE_2 and COX-2 ($r = 0.649$, $p < 0.01$).

3.3. Regulative effect of PMW on preadipocyte differentiation and adipocyte adipogenesis

The anti-adipogenic potential of PMW was first evaluated during the period of preadipocyte differentiation. Under obese conditions, it is desired to decrease the preadipocyte-adipocyte transition to reduce body fat mass. As determined by Oil Red O staining, after completion of the differentiation period, PMW decreased the intracellular lipid content by 8.5–56.0%, when compared to the NC (Fig. 4A). This lipid-lowering effect could be either due to the inhibition of cell proliferation or suppression of the preadipocyte adipogenesis (differentiation). It is known that obesity occurs as a consequence of a chronic imbalance between energy intake (lipogenesis) and energy expenditure (lipolysis). Further, the impact of PMW on lipogenesis/lipolysis in mature adipocytes was assessed and results are shown in Fig. 4B and C. Upon a 24-h treatment, PMW down-modulated the TG content in mature adipocytes by 12.9–55.9%, being consistent with the Oil red O results (TG content *vs.* Oil red O, $r = 0.418$, $p < 0.05$). On the other hand, the glycerol release was stimulated by specific PMW (1–9, 11–12, 14, 16, and 18–20) from 8.8 to 151.2%, when compared to the NC (TG content *vs.* glycerol release, $r = -0.556$, $p < 0.05$). Aberrant lipolysis might lead to higher circulating levels of free fatty acids (FA), which is closely associated with metabolic disorders. Whereas, activating lipolysis in adipocytes did not alter plasma FA levels in a high-fat diet-fed mouse model; in contrast, a promotion in FA oxidation and leanness was observed (Jaworski et al., 2009), implying that an "accurate" induction of adipocyte lipolysis can be a promising anti-adipogenic action of phenolic-rich foods.

Further evaluation on the expression level of peroxisome proliferator-activated receptor γ (PPARγ), a master coordinator of differentiation, revealed that specific PMW (1–4, 8–10, and 13–16) statistically blocked preadipocyte differentiation via inhibiting the PPARγ-mediated adipogenesis (Fig. 4D and E). This is in accordance with our previous findings that anthocyanins from purple maize dose-dependently suppressed PPARγ expression throughout the 3T3-L1 preadipocyte differentiation (Luna-Vital et al., 2017). Furthermore, the expression level of fatty acid synthase (FAS), a crucial enzyme involved in lipogenesis, was also down-modulated by certain PMW, with PMW_3, PMW_{14-16} and PMW_{20} showing the highest inhibitory potency.

3.4. Inhibitory potential of PMW on key enzymes related to T2DM and their insulin-sensitizing effect in insulin-resistant 3T3-L1 adipocytes

The inhibitory effects of PMW against key enzymes linked to T2DM were evaluated, namely, α-amylase and DPP-IV, and the results are given in Fig. 5A and B. PMW exhibited potential inhibition against α-amylase with IC_{50} values from 109.5 to 172.7 μg/mL. In the human digestive tract, pancreatic α-amylase is involved in the breakdown of oligo- and di-saccharides into absorbable mono-saccharides. Inhibition of this enzyme can be beneficial to T2DM by controlling the post-prandial blood glucose excursion. Moreover, PMW repressed DPP-IV activity with IC_{50} values ranging from 65.5 to 702.7 μg/mL. DPP-IV is a serine aminopeptidase that can inactivate the incretin hormone glucagon-like peptide-1, and it is currently among the pharmaceutical targets for regulating T2DM (Lacroix & Li-Chan, 2016). When comparing our results with those registered in the literature, the IC_{50} values of PMW are much lower (more potent) than those reported for the phenolic extracts from fig fruits ($IC_{50,\ \alpha\text{-amylase}}$ = 3.58–17.3 mg/mL) (Wojdyło et al., 2016), soybeans ($IC_{50,\ \alpha\text{-amylase}}$ = 320.5–526.3 μg/mL) (Ademiluyi & Oboh, 2013) and Brazilian native plants ($IC_{50,\ DPP\text{-}IV}$ >

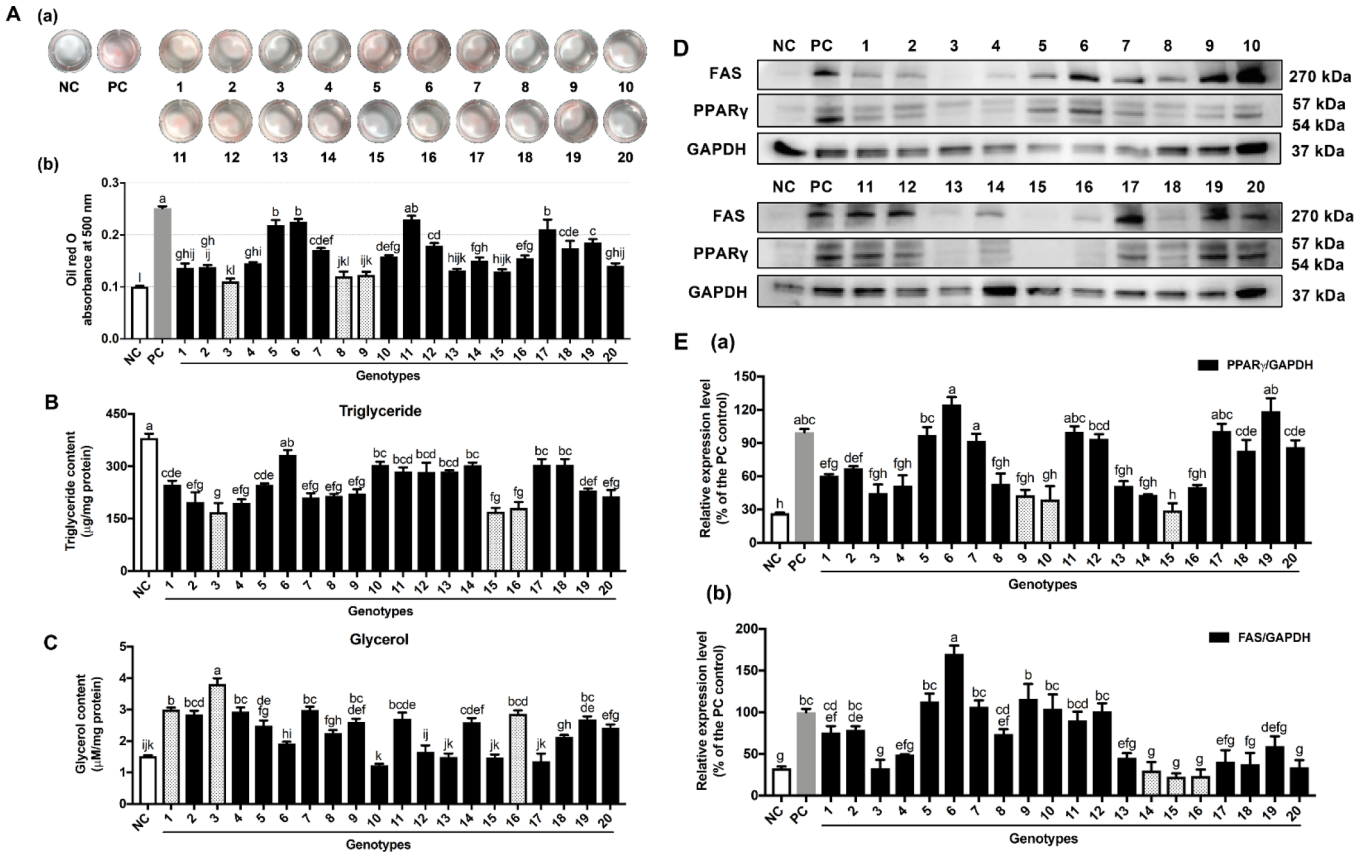

Fig. 4. Impact of PMW on (A) Intracellular lipid content, (B) Intracellular triglyceride content, (C) Extracellular glycerol release, and (D)-(E) PPARγ and FAS expression in 3T3-L1 adipocytes. For lipid content assessment, PPARγ, and FAS expression, 3T3-L1 preadipocytes were induced to differentiation incorporating 1.0 mg/mL of each PMW in the culture media, until Day 10, when the cells were stained with Oil Red O or lysed and analyzed for immunoblotting. As for triglyceride and glycerol assays, mature 3T3-L1 adipocytes were treated with 1 mg/mL of each PMW for 24 h. Values are expressed as the mean ± SD from three independent replicates in (A)-(C), and two independent replicates in (D)-(E). Bars with different letters indicate statistical difference ($p < 0.05$, Tukey's test) and the three most effective genotypes are filled with spotted pattern. (For interpretation of the references to color in this figure legend, the reader is referred to the web version of this article.)

0.71 mg/mL) (Oliveira, Araújo, Eidenberger, & Brandão, 2018). Colored maize pericarp can be precursors of beneficial food ingredients with hypoglycemic effects.

One of the major consequences of obesity-associated inflammation is insulin resistance. Further, we evaluated the insulin-sensitizing effect of PMW in 3T3-L1 adipocytes under a TNF-α-dependent inflammatory status. Superfluous generation of ROS is considered as a culprit in the development of T2DM (Kusminski et al., 2016) and anthocyanins and phenolics are known as free radical scavengers. Not surprisingly, PMW diminished the ROS level in insulin-resistant adipocytes by 29.7–64.2% (Fig. 5C). Moreover, the insulin-mediated glucose uptake was statistically reduced in TNF-α-induced adipocytes ($p < 0.05$), whereas PMW restored this blunted glucose uptake in insulin-resistant adipocytes by 30.3–139.1%, with PMW_{18} showing the best sensitizing effect, followed by PMW_4, PMW_{16}, and PMW_{19}, respectively (Fig. 5D).

3.5. Principal component analysis (PCA)

PCA was applied on standardized results to associate the phenolic components in PMW with their anti-inflammatory, anti-adipogenic and anti-diabetic properties. Score plot of PC1 *vs.* PC2 is shown in Fig. 6A; Pearson correlation matrix is presented as a heat map and shown in Fig. 6B. Supplementary Figure S4 indicates sample positioning and clustering, and Supplementary Table S7 presents eigenvalue of principal components (PCs) and factor loadings. As suggested by Field (2009), only the factor loading with absolute value > 0.4 was considered, representing 16% of the total variation. The leptin secretion was not included since non-statistical variations existed among genotypes.

The first five PCs explained 69.3% of the total variability. PC1, PC2 and PC3 represented 29.6%, 15.4% and 11.0% of the total variation, respectively. For anti-inflammatory properties, PC1 negatively correlated TNF-α, while positively associated with adiponectin, TAC, TPC, C3G, C3G-Mal, P3G, P3G-Mal, condensed dimer, phenolic acids, rutin, quercetin, and luteolin. NO, MCP-1, and iNOS expression can be explained by PC2, which was negatively linked to condensed dimer, *o*-coumaric acid, caffeic acid, vanillic acid and quercetin. IL-6 was defined by PC3 and strongly associated with Pr3G and Pr3G-Mal. Howbeit, for PGE_2 and COX-2 (factor loadings correlated with PC5), relatively weak correlations were observed between their values and phenolic components, implying that a more complicated mechanism was involved. Wang et al. (2015) compared the anti-inflammatory efficacy of 8 pear varieties in a xylene-induced mouse ear swelling model and concluded that flavonoids were the dominant anti-inflammatory components in the extracts. Indeed, a variety of dietary flavonoids, like anthocyanidins, flavones (luteolin), flavanones (naringenin), flavonols (quercetin, kaempferol) and their glycoside forms (rutin) have been recognized as anti-inflammatory agents with inhibitory effects on pro-inflammatory mediator production *in vitro* (González-Gallego et al., 2014). On the other hand, the condensed dimer, identified as catechin-cyanidin-3,5-diglucoside was a proanthocyanin present in colored maize and grape. In our previous study, the proanthocyanin fraction isolated from PMW down-regulated inflammatory changes in TNF-α-induced 3T3-L1 adipocytes (Luna-Vital et al., 2017).

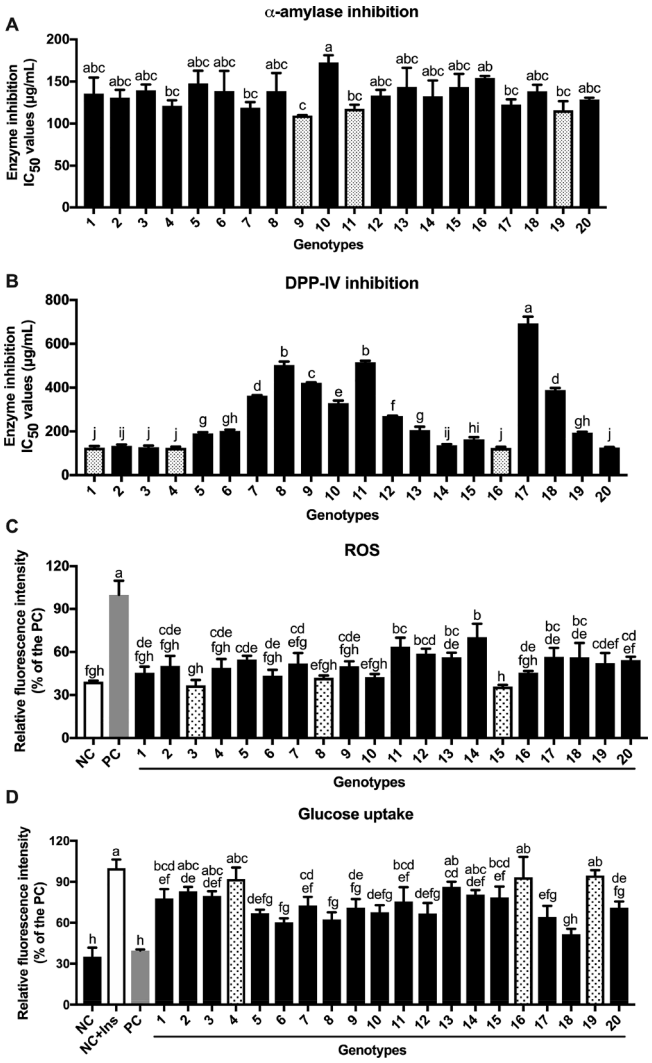

Fig. 5. Inhibition of PMW on (A) Biochemical determination of α-amylase and (B) Biochemical determination of DPP-IV activity, and impact of PMW on (C) *In vitro* intracellular ROS generation, and (D) *In vitro* glucose uptake in insulin-resistant 3T3-L1 adipocytes. For ROS and glucose uptake, insulin-resistant 3T3-L1 adipocytes were treated with 1.0 mg/mL of each PMW along with 10 ng/mL TNF-α for 24 h. Values are expressed as the mean ± SD from three independent replicates. Bars with different letters indicate statistical difference ($p < 0.05$, Tukey's test) and the three most effective genotypes are filled with spotted pattern.

With respect to anti-adipogenic potential, C3G, C3G-Mal, P3G, P3G-Mal, quercetin, luteolin and phenolic acids, especially, vanillic acid and protocatechuic acid, contributed to a better performance in inhibiting the preadipocyte-adipocyte transition (in terms of lipid accumulation, PPARγ and FAS expression) (Fig. 6B). Several phenolic extracts rich in C3G have been reported with anti-adipogenic effect in adipocytes via regulation of the PPARγ pathway, like those from bilberry (Suzuki et al., 2011) and black soybean (Kim et al., 2012). In addition, Mosqueda-Solís et al. (2017) compared the anti-adipogenic potential of fifteen phenolic compounds in adipocytes (by determining lipid content and adipogenesis-related gene expression) and concluded that quercetin was one of the most qualified phenolics. Whereas, it seems like naringenin is a potential PPARγ agonist here since a positive correlation was observed between its content and the PPARγ expression (loading factors correlate with PC1). Interestingly, in previous literature, naringenin was portrayed as both PPARγ agonist and antagonist (Mosqueda-Solís et al., 2017; Yoshida et al., 2013), indicating that selective modulation mechanisms can be involved. As for the lipid homeostasis in mature adipocytes, anthocyanins and rutin are more potent than other phenolics in down-regulating lipogenesis/up-regulating lipolysis in mature adipocytes. Moreover, it is worth noting that although a positive link exists between glycerol release and MCP-1, it does not indicate a pro-inflammatory effect of enhanced lipolysis, since MCP-1 was evaluated in inflamed adipocytes while the glycerol level was assayed under a basal condition.

Regarding anti-diabetic property, higher amounts of TAC, C3G, C3G-Mal, P3G, P3G-Mal, luteolin and rutin were associated with better capacity in modulating DPP-IV activity, ROS generation, and glucose uptake. Fan, Johnson, Lila, Yousef, and de Mejia (2013) reported that anthocyanins and flavonoids present in berry wine exhibited DPP-IV inhibitory effects. Computational docking further indicated that both C3G and luteolin could inactivate DPP-IV enzyme via binding with the active sites, showing similar binding modes with diprotin A, a potent DPP-IV inhibitor. However, rutin, a glycoside of quercetin, was portrayed by Fan et al. (2013) with no inhibition on DPP-IV. This discrepancy might be due to the differences in experimental conditions and analytical methods. As for the α-amylase inhibition, a lack of "composition-activity" relationship was observed, suggesting that other phenolic substances might play a part, for instance, other tannin-like compounds. McDougall reported that after removing soluble tannins from strawberry extracts, their α-amylase inhibitory activity was dramatically diminished (McDougall et al., 2005). On the other hand, C3G was considered as the major component that contributed to the insulin-sensitizing effects of several anthocyanin-rich extracts in cultured adipocytes and in rodent models (Luna-Vital et al., 2017; Guo et al., 2012). Whereas, limited information is available with regard to P3G. Our results might open up possibilities for plants rich in P3G and derivatives as promising hyperglycemia ingredients.

Upon clustering, the 20 maize genotypes were divided into three groups. Group 1, including genotype 1–4, was located on the upper right side and was characterized with high contents of C3G, C3G-Mal, P3G, P3G-Mal, luteolin and rutin, and better anti-adipogenic and anti-diabetic properties. Group 2 highlighted genotype 15 in the lower right corner, with high levels of phenolic acids and quercetin, and distinguished anti-inflammatory and anti-adipogenic efficacy. Group 3, containing all the remaining genotypes (5–14, 16–20), was clustered on the left half of the plot and showed less prominent biological effects. As such, based on the intended uses, proper genotypes can be selected and cultivated for further commercial applications.

4. Conclusions

In conclusion, the 20 purple maize genotypes exhibited a wide range of phenolic compounds, including phenolic acids, anthocyanins, flavonols, flavons, among others. Considerable differences were also observed among genotypes in terms of their anti-inflammatory, anti-adipogenic and anti-diabetic properties. By using multivariate analysis, it was concluded that C3G, P3G and their acylated forms contributed to the biological activities of PMW. Quercetin, luteolin and rutin were the primary anti-inflammatory and anti-diabetic compounds; while vanillic acid and protocatechuic acid contributed to the anti-adipogenic potential of PMW. Overall, our results provide useful information to select or develop colored maize genotypes with added-value, supporting the hypothesis of the use of colored maize pigments as ingredients in functional foods. A summary illustrating the molecular mechanism of the targeted parameters in macrophages and adipocytes is given in Supplementary Figure S5. To our knowledge, this is the first study comprehensively investigating the composition-bioactivity relationship of dietary phenolics from colored maize towards inflammation, adipogenesis and glucose homeostasis *in vitro*. Future studies using *in vivo* models are required to confirm the biological effect of selected maize genotypes.

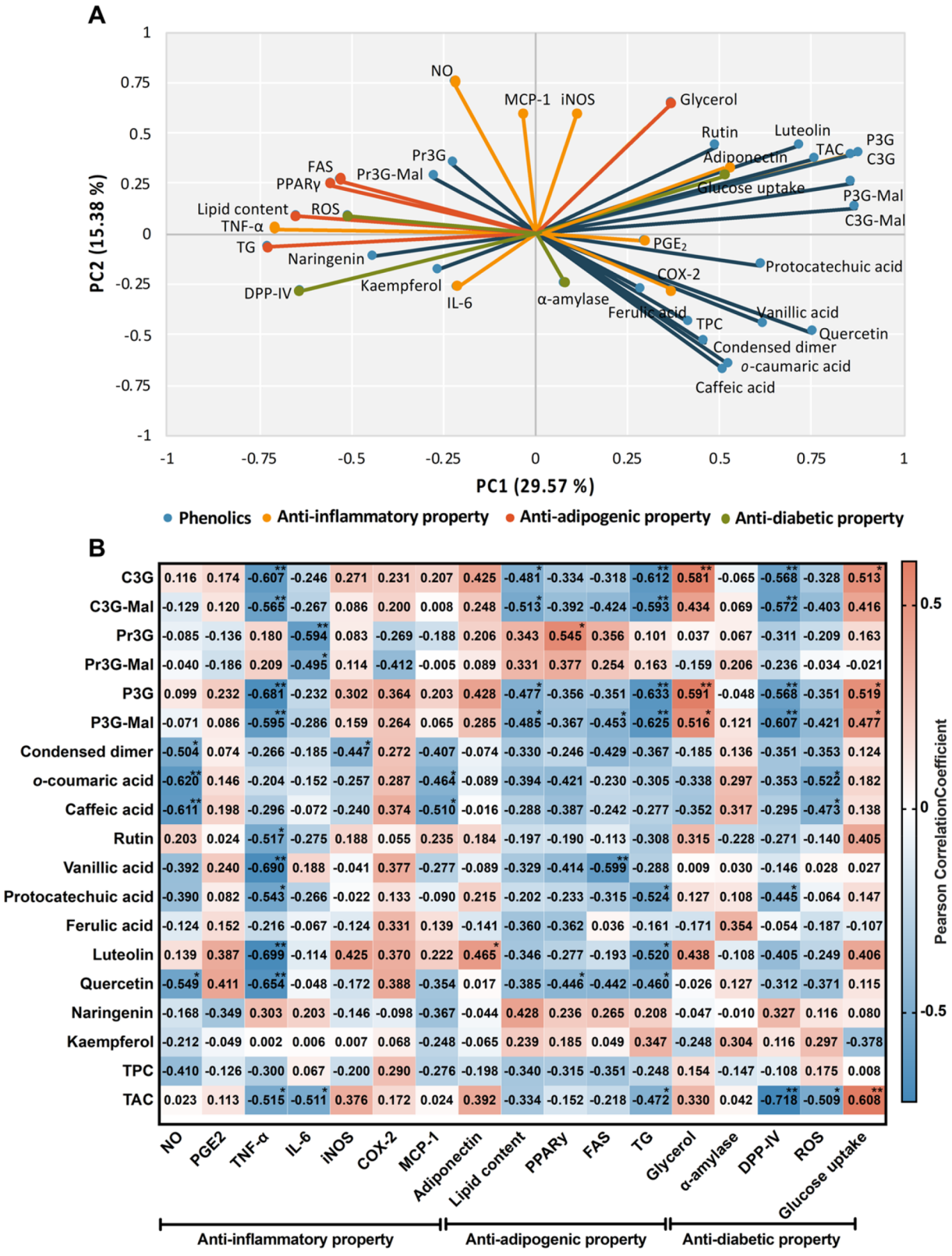

Fig. 6. (A) Principal component analysis showing associations between phenolic composition and anti-inflammatory, anti-adipogenic, and anti-diabetic properties. PC1 (x) *vs.* PC2 (y) was presented. (B) Heat map of the Pearson correlation coefficients. *significant at the 0.05 level ($p < 0.05$); **significant at the 0.01 level ($p < 0.01$). C3G, cyanidin-3-*O*-glucoside; Pr3G, pelargonidin-3-*O*-glucoside; P3G, peonidin-3-*O*-glucoside; C3G-Mal, cyanidin-3-(6′-malonylglucoside); Pr3G-Mal, pelargonidin-3-(6′-malonylglucoside); P3G-Mal, peonidin-3-(6′-malonylglucoside); Condensed dimer was identified as catechin-cyanidin-3,5-diglucoside.

Conflict of interest

The authors declare that they have no conflicts of interest.

Acknowledgment

This project was financially supported by USDA-NIFA-HATCH project 1014457. Q.Z.Z thank China Scholarship Council (201706610006) for studying fellowship and travel aid.

Appendix A. Supplementary data

Supplementary data to this article can be found online at https://doi.org/10.1016/j.foodchem.2019.03.116.

References

Ademiluyi, A. O., & Oboh, G. J. E. (2013). Soybean phenolic-rich extracts inhibit key-enzymes linked to type 2 diabetes (α-amylase and α-glucosidase) and hypertension (angiotensin I converting enzyme) in vitro. *Experimental and Toxicologic Pathology, 65*(3), 305–309.

Alonso-Castro, A. J., & Salazar-Olivo, L. A. (2008). The anti-diabetic properties of *Guazuma ulmifolia* Lam are mediated by the stimulation of glucose uptake in normal and diabetic adipocytes without inducing adipogenesis. *Journal of Ethnopharmacology, 118*(2), 252–256.

Bower, A. M., Real Hernandez, L. M., Berhow, M. A., & de Mejia, E. G. (2014). Bioactive compounds from culinary herbs inhibit a molecular target for type 2 diabetes management, dipeptidyl peptidase IV. *Journal of Agricultural and Food Chemistry, 62*(26), 6147–6158.

Chen, C., Somavat, P., Singh, V., & de Mejia, E. G. (2017). Chemical characterization of proanthocyanidins in purple, blue, and red maize coproducts from different milling processes and their anti-inflammatory properties. *Industrial crops and products, 109*, 464–475.

Chen, L., Yang, M., Mou, H., & Kong, Q. (2018). Ultrasound-assisted extraction and characterization of anthocyanins from purple corn bran. *Journal of Food Processing and Preservation, 42*, e13377.

Chatham, L. A., West, L., Berhow, M. A., Vermillion, K. E., & Juvik, J. A. (2018). Unique flavanol-anthocyanin condensed forms in Apache red purple corn. *Journal of Agricultural and Food Chemistry, 66*(41), 10844–10854.

Cuevas-Montilla, E., Hillebrand, S., Antezana, A., & Winterhalter, P. (2011). Soluble and bound phenolic compounds in different Bolivian purple corn (Zea mays L.) cultivars. *Journal of Agricultural and Food Chemistry, 59*(13), 7068–7074.

Fan, J., Johnson, M. H., Lila, M. A., Yousef, G., & de Mejia, E. G. (2013). Berry and citrus phenolic compounds inhibit dipeptidyl peptidase IV: Implications in diabetes management. *Evidence-Based Complementary and Alternative Medicine, 2013*, 1–13. https://doi.org/10.1155/2013/479505.

Field, A. (2009). *Discovering statistics using SPSS*. Sage publications.

González-Gallego, Javier, García-Mediavilla, Maria Victoria, Sánchez-Campos, Sonia, & Tuñón, María J. (2014). *Polyphenols in Human Health and Disease* (pp. 435–452). Elsevier. https://doi.org/10.1016/B978-0-12-398456-2.00032-3.

Guo, H., Xia, M., Zou, T., Ling, W., Zhong, R., & Zhang, W. (2012). Cyanidin 3-glucoside attenuates obesity-associated insulin resistance and hepatic steatosis in high-fat diet-fed and db/db mice via the transcription factor FoxO1. *The Journal of Nutritional Biochemistry, 23*(4), 349–360.

Haggard, S., Luna-Vital, D., West, L., Juvik, J. A., Chatham, L., Paulsmeyer, M., & de Mejia, E. G. (2018). Comparison of chemical, color stability, and phenolic composition from pericarp of nine colored corn unique varieties in a beverage model. *Food Research International, 105*, 286–297.

Harakotr, B., Suriharn, B., Tangwongchai, R., Scott, M. P., & Lertrat, K. (2014). Anthocyanin, phenolics and antioxidant activity changes in purple waxy corn as affected by traditional cooking. *Food Chemistry, 164*, 510–517.

Hsu, C. L., & Yen, G. C. (2006). Induction of cell apoptosis in 3T3-L1 pre-adipocytes by flavonoids is associated with their antioxidant activity. *Molecular Nutrition & Food Research, 50*(11), 1072–1079.

Hu, Q., & Xu, J. (2011). Profiles of carotenoids, anthocyanins, phenolics, and antioxidant activity of selected color waxy corn grains during maturation. *Journal of Agricultural and Food Chemistry, 59*(5), 2026–2033.

Jaworski, K., Ahmadian, M., Duncan, R. E., Sarkadi-Nagy, E., Varady, K. A., Hellerstein, M. K., ... De Val, S. (2009). AdPLA ablation increases lipolysis and prevents obesity induced by high-fat feeding or leptin deficiency. *Nature Medicine, 15*(2), 159.

Kanda, H., Tateya, S., Tamori, Y., Kotani, K., Hiasa, K. I., Kitazawa, R., ... Kasuga, M. (2006). MCP-1 contributes to macrophage infiltration into adipose tissue, insulin resistance, and hepatic steatosis in obesity. *The Journal of Clinical Investigation, 116*(6), 1494–1505.

Kim, H. K., Kim, J. N., Han, S. N., Nam, J. H., Na, H. N., & Ha, T. J. (2012). Black soybean anthocyanins inhibit adipocyte differentiation in 3T3-L1 cells. *Nutrition Research, 32*(10), 770–777.

Kusminski, C. M., Bickel, P. E., & Scherer, P. E. (2016). Targeting adipose tissue in the treatment of obesity-associated diabetes. *Nature Reviews Drug Discovery, 15*(9), 639.

Lacroix, I. M., & Li-Chan, E. C. (2016). Food-derived dipeptidyl-peptidase IV inhibitors as a potential approach for glycemic regulation–Current knowledge and future research considerations. *Trends in Food Science & Technology, 54*, 1–16.

Lao, F., & Giusti, M. M. (2016). Quantification of purple corn (Zea mays L.) anthocyanins using spectrophotometric and HPLC approaches: Method comparison and correlation. *Food Analytical Methods, 9*(5), 1367–1380.

Lee, J., Durst, R. W., & Wrolstad, R. E. (2005). Determination of total monomeric anthocyanin pigment content of fruit juices, beverages, natural colorants, and wines by the pH differential method: Collaborative study. *Journal of AOAC International, 88*(5), 1269–1278.

Li, D., Wang, P., Luo, Y., Zhao, M., & Chen, F. (2017). Health benefits of anthocyanins and molecular mechanisms: Update from recent decade. *Critical Reviews in Food Science and Nutrition, 57*(8), 1729–1741.

Li, Q., Somavat, P., Singh, V., Chatham, L., & de Mejia, E. G. (2017). A comparative study of anthocyanin distribution in purple and blue corn coproducts from three conventional fractionation processes. *Food Chemistry, 231*, 332–339.

Luna-Vital, D., Weiss, M., & Gonzalez de Mejia, E. (2017). Anthocyanins from Purple Corn Ameliorated Tumor Necrosis Factor-α-Induced Inflammation and Insulin Resistance in 3T3-L1 Adipocytes via Activation of Insulin Signaling and Enhanced GLUT4 Translocation. *Molecular Nutrition & Food Research, 61*(12), 1700362.

Luna-Vital, D., Li, Q., West, L., West, M., & de Mejia, E. G. (2017). Anthocyanin condensed forms do not affect color or chemical stability of purple corn pericarp extracts stored under different pHs. *Food Chemistry, 232*, 639–647.

Mancuso, C., & Santangelo, R. (2014). Ferulic acid: Pharmacological and toxicological aspects. *Food and Chemical Toxicology, 65*, 185–195.

Mazewski, C., Liang, K., & de Mejia, E. G. (2017). Inhibitory potential of anthocyanin-rich purple and red corn extracts on human colorectal cancer cell proliferation in vitro. *Journal of Functional Foods, 34*, 254–265.

McDougall, G. J., Shpiro, F., Dobson, P., Smith, P., Blake, A., & Stewart, D. (2005). Different polyphenolic components of soft fruits inhibit α-amylase and α-glucosidase. *Journal of Agricultural and Food Chemistry, 53*(7), 2760–2766.

Min, S. W., Ryu, S. N., & Kim, D. H. (2010). Anti-inflammatory effects of black rice, cyanidin-3-O-β-D-glycoside, and its metabolites, cyanidin and protocatechuic acid. *International Immunopharmacology, 10*(8), 959–966.

Mohamed, S. (2014). Functional foods against metabolic syndrome (obesity, diabetes, hypertension and dyslipidemia) and cardiovascular disease. *Trends in Food Science & Technology, 35*(2), 114–128.

Monroy, Y. M., Rodrigues, R. A. F., Sartoratto, A., & Cabral, F. A. (2016). Extraction of bioactive compounds from cob and pericarp of purple corn (*Zea mays* L.) by sequential extraction in fixed bed extractor using supercritical CO_2, ethanol, and water as solvents. *The Journal of Supercritical Fluids, 107*, 250–259.

Mosqueda-Solís, A., Lasa, A., Gómez-Zorita, S., Eseberri, I., Picó, C., & Portillo, M. P. (2017). Screening of potential anti-adipogenic effects of phenolic compounds showing different chemical structure in 3T3-L1 preadipocytes. *Food & Function, 8*(10), 3576–3586.

Mraz, M., & Haluzik, M. (2014). The role of adipose tissue immune cells in obesity and low-grade inflammation. *Journal of Endocrinology*, JOE-14.

Oliveira, V. B., Araújo, R. L., Eidenberger, T., & Brandão, M. G. (2018). Chemical composition and inhibitory activities on dipeptidyl peptidase IV and pancreatic lipase of two underutilized species from the Brazilian Savannah: Oxalis cordata A. St.-Hil. and Xylopia aromatica (Lam.) Mart. *Food Research International, 105*, 989–995.

Paulsmeyer, M., Chatham, L., Becker, T., West, M., West, L., & Juvik, J. (2017). Survey of anthocyanin composition and concentration in diverse maize germplasms. *Journal of Agricultural and Food Chemistry, 65*(21), 4341–4350.

Prior, R. L., & Wu, X. (2006). Anthocyanins: Structural characteristics that result in unique metabolic patterns and biological activities. *Free Radical Research, 40*(10), 1014–1028.

Suzuki, R., Tanaka, M., Takanashi, M., Hussain, A., Yuan, B., Toyoda, H., & Kuroda, M. (2011). Anthocyanidins-enriched bilberry extracts inhibit 3T3-L1 adipocyte differentiation via the insulin pathway. *Nutrition & Metabolism, 8*(1), 14.

Wang, T., Li, X., Zhou, B., Li, H., Zeng, J., & Gao, W. (2015). Anti-diabetic activity in type 2 diabetic mice and α-glucosidase inhibitory, antioxidant and anti-inflammatory potential of chemically profiled pear peel and pulp extracts (Pyrus spp.). *Journal of Functional Foods, 13*, 276–288.

Weisberg, S. P., McCann, D., Desai, M., Rosenbaum, M., Leibel, R. L., & Ferrante, A. W. (2003). Obesity is associated with macrophage accumulation in adipose tissue. *The Journal of Clinical Investigation, 112*(12), 1796–1808.

Wojdyło, A., Nowicka, P., Carbonell-Barrachina, Á. A., & Hernández, F. (2016). Phenolic compounds, antioxidant and antidiabetic activity of different cultivars of Ficus carica L. fruits. *Journal of Functional Foods, 25*, 421–432.

World Health Organization. (2017). Fact Sheet: Obesity and Overweight, 2015. 29(09).

Yang, J. Y., Della-Fera, M. A., Rayalam, S., Ambati, S., Hartzell, D. L., Park, H. J., & Baile, C. A. (2008). Enhanced inhibition of adipogenesis and induction of apoptosis in 3T3-L1 adipocytes with combinations of resveratrol and quercetin. *Life Sciences, 82*(19–20), 1032–1039.

Yang, Z., & Zhai, W. (2010). Optimization of microwave-assisted extraction of anthocyanins from purple corn (Zea mays L.) cob and identification with HPLC–MS. *Innovative Food Science and Emerging Technologies, 11*, 470–476.

Yoshida, H., Watanabe, W., Oomagari, H., Tsuruta, E., Shida, M., & Kurokawa, M. (2013). Citrus flavonoid naringenin inhibits TLR2 expression in adipocytes. *The Journal of Nutritional Biochemistry, 24*(7), 1276–1284.

Zebisch, K., Voigt, V., Wabitsch, M., & Brandsch, M. (2012). Protocol for effective differentiation of 3T3-L1 cells to adipocytes. *Analytical Biochemistry, 425*(1), 88–90.

Zhao, X., Corrales, M., Zhang, C., Hu, X., Ma, Y., & Tauscher, B. (2008). Composition and thermal stability of anthocyanins from Chinese purple corn (*Zea mays* L.). *Journal of Agricultural and Food Chemistry, 56*(22), 10761–10766.

Žilić, S., Serpen, A., Akıllıoğlu, G., Gökmen, V., & Vančetović, J. (2012). Phenolic compounds, carotenoids, anthocyanins, and antioxidant capacity of colored maize (Zea mays L.) kernels. *Journal of Agricultural and Food Chemistry, 60*(5), 1224–1231.